

# Non-Fermi liquid and topological states with strong spin-orbit coupling

Eun-Gook Moon,<sup>1</sup> Cenke Xu,<sup>1</sup> Yong Baek Kim,<sup>2</sup> and Leon Balents<sup>3</sup>

<sup>1</sup>*Department of Physics, University of California, Santa Barbara, CA 93106, USA*

<sup>2</sup>*Department of Physics, University of Toronto, Toronto, Ontario M5S 1A7, Canada*

<sup>3</sup>*Kavli Institute for Theoretical Physics, University of California, Santa Barbara, CA 93106, USA*

(Dated: September 19, 2018)

We argue that a class of strongly spin-orbit coupled materials, including some pyrochlore iridates and the inverted band gap semiconductor HgTe, may be described by a minimal model consisting of the Luttinger Hamiltonian supplemented by Coulomb interactions, a problem studied by Abrikosov and collaborators. It contains two-fold degenerate conduction and valence bands touching quadratically at the zone center. Using modern renormalization group methods, we update and extend Abrikosov’s classic work and show that interactions induce a quantum critical non-Fermi liquid phase, stable provided time-reversal and cubic symmetries are maintained. We determine the universal power-law exponents describing various observables in this “Luttinger Abrikosov Beneslavskii” state, which include conductivity, specific heat, non-linear susceptibility and magnetic Gruneisen number. Furthermore, we determine the phase diagram in the presence of cubic and/or time-reversal symmetry breaking perturbations, which includes topological insulator and Weyl semi-metal phases. Many of these phases possess an extraordinarily large anomalous Hall effect, with the Hall conductivity scaling *sub-linearly* with magnetization,  $\sigma_{xy} \sim M^{0.51}$ .

Divining the nature of critical non-Fermi liquid (NFL) phases of electrons is one of the most outstanding problems in correlated electron systems, such as cuprates, pnictides, and heavy fermion materials [1–4]. Theory, spurred largely by NFL behavior in the cuprates, has focused on models with large Fermi surfaces, appropriate to these materials. Though there have been promising technical advances[5], this approach has not provided clear resolution of experimental puzzles. Recent theory and experiment have uncovered a new frontier for correlated phenomena: Mott correlation physics in materials with strong spin-orbit coupling (SOC) [6, 7]. Of particular interest in this regard are the 5d transition metal oxides, where compelling evidence has been built for Mott phenomena driven cooperatively by SOC and Coulomb interactions [6–8]. Here we consider the possibility of distinct NFL states in the strong SOC regime.

We are particularly motivated by the pyrochlore iridates,  $A_2Ir_2O_7$ , where A is a lanthanide element [9, 10]. These materials display  $T > 0$  metal-insulator transitions, with the metal-insulator transition temperature decreasing with increasing A radius. The progression culminates with  $Pr_2Ir_2O_7$ , which is a highly unconventional metal down to the lowest temperatures [11, 12]. It displays logarithmic NFL behavior of the magnetic susceptibility, and a remarkable enormous zero field anomalous Hall effect (AHE), in the absence of any measurable magnetization [11, 12].

With these studies as motivation, we utilize prior studies of the electronic structure of pyrochlore iridates[13–15] to show that a minimal description for the electronic states in their paramagnetic phase is a storied Hamiltonian from semiconductor physics: the Luttinger model of inverted band gap semiconductors [16]. This model has gained recent notoriety for its relevance to HgTe, the

starting material for some topological insulators [17–20]. While HgTe is a weakly correlated material where band structure alone provides a sufficient description, in the 5d materials the Luttinger Hamiltonian must be supplanted by interactions.

In this paper, we carry out such an analysis, rediscovering and extending a storied analysis by Abrikosov and Beneslavskii of Coulomb forces on the Luttinger problem [21, 22]. Using modern renormalization group (RG) techniques, we confirm Abrikosov’s conclusion that long-range Coulomb interactions convert the quadratic band touching into a quantum critical NFL, prove the stability of the state within an  $\epsilon$  expansion, and calculate the full set of anomalous dimensions characterizing the state. Consequently, we call the resulting phase a *Luttinger-Abrikosov-Beneslavskii* (LAB) state. While the LAB phase is stable in the presence of time-reversal and cubic symmetries, we show that it is a “parent” state for other exotic states that can be reached by breaking either or both of these: metallic and double-Weyl semi-metallic phases with enormous anomalous Hall effects (AHEs), and topological insulators. We discuss the implications for the iridates at the end of the paper.

The LAB phase itself has striking properties. Its NFL nature is revealed directly by algebraic singularities in the electron spectral function (probed in angle-resolved photoemission) and in optical conductivity, as well as indirectly through many power law thermodynamic and response functions.

We now turn to the exposition of these results. We consider the *paramagnetic* band structure based on prior work [13–15], which argued that the states at the zone center ( $\Gamma$  point) near the Fermi energy are comprised of the four-dimensional representation, which can be described by “angular momentum” operators  $\vec{J}$  (which are

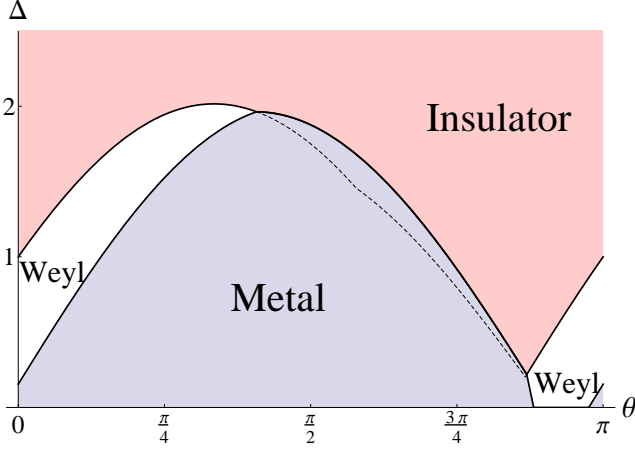


FIG. 1. Phase diagram of the perturbed LAB in the space of renormalized strain to Zeeman field ratio,  $\Delta \equiv (\delta/H)_R$ , versus cubic Zeeman angle,  $\theta$ . Here “Weyl” denotes the (double) Weyl semimetal, “Ins.” insulator, and “Metal” a metallic phase which has Weyl points shifted from the Fermi energy in the region below the dashed line. For  $H = 0$ , the insulator is a topological insulator.

$j = 3/2$  matrices) transforming as the  $T_2$  representation of the cubic group. In our minimal model, we assume only these states close to  $\Gamma$  are important. Then  $k \cdot p$  theory and cubic symmetry determines the band structure in its vicinity to be precisely described by the Luttinger Hamiltonian with three effective mass parameters [16, 23],

$$\mathcal{H}_0(k) = \frac{k^2}{2\tilde{M}_0} + \frac{\frac{5}{4}k^2 - (\vec{k} \cdot \vec{J})^2}{2m} - \frac{(k_x^2 J_x^2 + k_y^2 J_y^2 + k_z^2 J_z^2)}{2M_c}.$$

This describes doubly degenerate bands with energy

$$E_{\pm}(k) = \frac{k^2}{2M_0} \pm \sqrt{\left(\frac{k^2}{2m}\right)^2 + \frac{m + 2M_c}{4mM_c^2} p_c(k)}, \quad (1)$$

where  $p_c(k) = \sum_i k_i^4 - \sum_{i \neq j} k_i^2 k_j^2$  and  $M_0 = (4M_c \tilde{M}_0)/(4M_c - 5\tilde{M}_0)$ . Henceforth we assume  $M_0 > m$ , which describes conduction and valence bands touching quadratically at  $E = k = 0$ , where the chemical potential for the undoped material crosses.

The LAB is obtained by adding to this the long-range Coulomb interaction. We implement the latter by a scalar potential  $\varphi$ , which in the Euclidean path integral formalism gives the action

$$S_L = \int d\tau d^d x \left\{ \psi^\dagger \left[ \partial_\tau - ie\varphi + \hat{\mathcal{H}}_0 \right] \psi + \frac{c_0}{2} (\partial_i \varphi)^2 \right\}, \quad (2)$$

with  $\hat{\mathcal{H}}_0 = \mathcal{H}_0(-i\vec{\nabla})$  and  $c_0 = 1/4\pi$ . Here  $\psi$  is a four-component spinor, but subsequently we will artificially add an additional  $U(N_f)$  flavor index, which allows a check on our calculations by large  $N_f$  methods; the physical case is  $N_f = 1$ . Eq. (2) contains in addition to the

three mass parameters, the Coulomb coupling constant  $e$ . For  $e = 0$ , scale invariance is manifest, with the scaling dimensions  $[x^{-1}] = 1$ ,  $[\tau^{-1}] = z$ ,  $[\psi] = \frac{d}{2}$ ,  $[\frac{1}{m}] = z - 2$ ,  $[\varphi] = (d + z - 2)/2$ . Here we introduce the dynamic critical exponent ( $z$ ), which is naturally  $z = 2$  with  $e = 0$ , but will become non-trivial with interactions.

Directly in the physical case  $d = 3$ , the dimension of the coupling constant is  $[e^2] = 1$ , so Coulomb interactions are strongly relevant. Therefore we employ the  $\varepsilon = 4 - d$  expansion to control the RG analysis. As familiar from quantum electrodynamics, three one loop Feynmann diagrams contribute to leading order in  $\varepsilon$ : the fermion self-energy, boson self-energy, and vertex correction. Here we show that the relevance of Coulomb interactions signals, rather than a flow to strong coupling and a symmetry breaking instability, the formation of a new *stable* interacting fixed point, which describes the critical non-Fermi liquid LAB state (Abrikosov’s analysis tacitly assumes this stability).

The RG is carried out perturbatively in  $e$ , but non-perturbatively in the mass parameters. Thus a full treatment gives non-trivial and complete beta functions for the two dimensionless mass ratios  $m/M_0$ ,  $m/M_c$ ; these are given in the Supplementary Material. The analysis of the full RG shows, however, that there is a single stable *isotropic* fixed point corresponding to  $m/M_0 = m/M_c = 0$ , so for simplicity we quote in the main text only the results in the vicinity of this point.

In this limit, the leading contribution to the bosonic self energy becomes

$$\frac{1}{N_f} \Sigma_\varphi(q, 0) = -(2m)e^2 \left[ \int \frac{d^d k}{(2\pi)^d} \frac{1}{k^4} \right] \times q^2, \quad (3)$$

where we took the  $\omega \rightarrow 0$  limit because frequency dependence is subdominant. The divergence should be absorbed by rescaling the bosonic field,  $\varphi \rightarrow e^{-\eta_b d\ell} \varphi$  upon reduction of the hard momentum cutoff  $\Lambda \rightarrow e^{-d\ell} \Lambda$ , which defines the RG parameter  $\ell$ . This gives the bosonic anomalous dimension  $\eta_b = 2N_f u$  [24], where the dimensionless coupling constant is  $u = \frac{m e^2}{8\pi^2 c_0 \Lambda^{4-d}}$ , which has the physical meaning in  $d = 3$  of the ratio of the real space cutoff to the effective Bohr radius. The frequency dependence of the one loop fermionic self-energy and the vertex correction both vanish, the result of a Ward identity. For  $k \neq 0$ , the fermion self-energy gives mass corrections, e.g.  $\delta(1/m) = 8u/(15m) \times d\ell$  to leading order. Detailed analysis is given in the Supplementary Material.

Given these calculations, we choose  $z = 2 - 8u/15$  to keep the mass  $m$  fixed, which gives the RG equations, to lowest order in  $m/M_c, m/M_0$ :

$$\begin{aligned} \frac{d}{d\ell} u &= \varepsilon u - \frac{30N_f + 8}{15} u^2, \\ \frac{d}{d\ell} \left( \frac{m}{M_c} \right) &= -0.152u \left( \frac{m}{M_c} \right), \quad \frac{d}{d\ell} \left( \frac{m}{M_0} \right) = -\frac{8}{15} u \left( \frac{m}{M_0} \right). \end{aligned} \quad (4)$$

From the first equation above we find the fixed point coupling and hence dynamical exponent,

$$u^* = \frac{15}{30N_f + 8}\varepsilon, \quad z = 2 - \frac{4}{15N_f + 4}\varepsilon, \quad (5)$$

and since  $u^* > 0$ , the second line in Eq. (4) implies both  $m/M_0$  and  $m/M_c$  are irrelevant. This establishes the existence and nature of the stable, isotropic fixed point describing the LAB phase. As a check, we have carried out a large  $N_f$  expansion, which gives the same bosonic anomalous dimension as in the  $\varepsilon$  expansion at the one-loop level, supporting the stability of the LAB phase.

The presence of the stable interacting fixed point can be understood physically as a balance of partial dynamical screening of the Coulomb interactions by electron-hole pairs and mass enhancement of the same quasiparticles by pairs. This situation is in sharp contrast to the case of a vanishing *indirect* band gap, for which to leading order in the long-range Coulomb interaction electrons and holes are separately conserved, so there is no screening by virtual electron-hole pairs, and exciton formation destabilizes the putative gapless state[25].

Using the RG, we can evaluate the anomalous dimension of any physical operator. By charge conservation,  $[\psi^\dagger\psi] = d$ . Due to the isotropy of the fixed point, there are only two non-trivial values for the other charge-conserving fermion bilinears. We obtain,  $[\psi^\dagger\Gamma_a\psi] = d + \eta_1$ ,  $[\psi^\dagger\Gamma_{ab}\psi] = d + \eta_{12}$ , where  $\Gamma_a$  are the (time-reversal invariant) Dirac gamma matrices,  $\Gamma_{ab} = -\frac{i}{2}[\Gamma_a, \Gamma_b]$  are time-reversal odd, and  $a, b = 1, 2, \dots, 5$ . Using the standard operator insertion technique, we find  $\eta_1 = -\frac{6}{15N_f + 4}\varepsilon$  and  $\eta_{12} = -\frac{3}{15N_f + 4}\varepsilon$ . These operators describe many physical observables, *e.g.* the “angular momentum” operator  $J_z \sim \psi^\dagger(-\Gamma_{34} - \frac{1}{2}\Gamma_{12})\psi$ . The negative anomalous dimension of these operators suggests the a schematic picture of power-law excitons due to electron-hole attraction. For pairing channels, we find positive anomalous dimensions, consistent with this view. The local pairing channel has  $\eta_{\text{pairing}} = \frac{u^*}{5} = \frac{3}{30N_f + 8}\varepsilon$ .

Using these results, we obtain thermodynamic responses such as the specific heat,  $c_v \sim T^{d/z} \approx T^{1.7}$  and the spin susceptibility  $\chi(T) \sim a + bT^{(d-z+2\eta_{12})/z} \approx a + bT^{0.5}$ , with some constants  $a, b$ . Interestingly, the non-linear susceptibility  $\chi_3 = \partial^3 M / \partial H^3|_{H=0} \sim T^{-(3z-4\eta_{12}-d)/z} \approx T^{-1.7}$  diverges, as in spin glasses but with completely different physics. Comparing the scaling of current and electric field gives the usual result  $[\sigma_{ij}] = d - 2$ . Consequently, the temperature and frequency dependence of the conductivity is  $\sigma(\omega, T) \sim T^{1/z} \mathcal{F}(\omega/T)$ , and a *clean, undoped* LAB is therefore a power-law insulator.

We now turn to the effect of applied strain and Zeeman field upon the LAB. These perturbations break cubic/time-reversal symmetries, and thus destabilize the LAB. Due to the isotropic nature of the LAB fixed point,

the response to the Zeeman field alone is to leading order independent of its direction (the cubic mass  $1/M_c$  can be “dangerously irrelevant”, however – see below), so we take it to lie along the (001) direction. We consider for simplicity tetragonal strain which preserves  $C_4$  rotation about this axis (in the absence of Zeeman field, the direction of strain is again unimportant). This leads to the perturbations

$$\mathcal{H}' = -\delta(J_z^2 - \frac{5}{4}) - H(\cos(\theta)J_z + \sin(\theta)J_z^3), \quad (6)$$

where  $\delta$  parametrizes the strain,  $h$  is the Zeeman field, and  $\theta$  controls the strength of the cubic Zeeman term allowed by the cubic symmetry [26, 27]. Using the RG results, the dimensions of these perturbations are  $[\delta] = z - \eta_1 \approx 2.1$  and  $[H] = z - \eta_{12} \approx 1.9$ ; *i.e.* strain is slightly enhanced while Zeeman field is slightly suppressed by interactions. However, both dimensions are positive and close to 2, so that they are strongly *relevant*. They flow to strong coupling under the RG, and the fate of the system must be re-analyzed in the limit.

To do so, we assume, and check self-consistently, that interactions have weak effects at strong coupling, and simply solve the quadratic Hamiltonian (with  $m/M_0 = m/M_c = 0$ ) in the presence of the renormalized  $\mathcal{H}'$ . The result depends upon the dimensionless quantities  $\theta$  and the renormalized coupling ratio  $\Delta = (\delta/H)_R \sim \delta/H^{(z-\eta_1)/(z-\eta_{12})}$ . For  $H = 0$  ( $\Delta = \infty$ ), we have time-reversal invariance, and we recover the known result that strain  $\delta > 0$  induces a gapped, 3d TI phase, as observed in HgTe [19]. The situation in applied Zeeman field is more interesting. Notice that for  $\vec{k} = k\hat{z}$ ,  $J_z$  is a good quantum number, and there is no level repulsion between bands of different  $J_z$ . This allows (non-degenerate) bands to cross along this axis, which indeed occurs when  $|\Delta|$  is not too large. Further analysis in the Supplementary Material shows that these crossings correspond to a pair of *double Weyl points*, with linear dispersion along the  $z$  axis and quadratic dispersion normal to it. These points are strength  $\pm 2$  monopoles in momentum space. Away from the  $k_z$  axis, electron and hole pockets may accidentally cross the Fermi energy. If this does not occur, one has a pristine double Weyl semimetal, which occurs for the angular range  $\theta_1 \leq \theta \leq \theta_2$ , where  $\theta_1 = -\tan^{-1}(\frac{8+4\sqrt{3}}{7\sqrt{3}+26})$  and  $\theta_2 = \tan^{-1}(\frac{8-4\sqrt{3}}{7\sqrt{3}-26})$  for  $\delta = 0$ , as shown in horizontal axis of Fig. 1. When  $0 < |\Delta| < \infty$ , we observe insulating, double Weyl semimetal, and Weyl metal (with coexisting electron-hole pockets) phases, as shown in Figure 1. Note that in all these phases, the Coulomb interactions become either unimportant (in the insulator), screened (in the metal), or marginally irrelevant (in the Weyl semimetal), justifying our treatment of the phase diagram to a first approximation.

More subtle effects may make small modifications to this picture. Coulomb interactions can destabilize some

of the quantum phase transitions in Figure 1, leading to intermediate phases. When the magnetic field is applied along a low symmetry axis, the double Weyl points can split into multiple single Weyl points, once the effects of the cubic mass  $1/M_c$  is included, which is dangerously irrelevant in this case.

A striking experimental consequence of this phase diagram is the AHE due to the Zeeman field, which could originate either from an external magnetic field or as an exchange field due to local moments in the material. The latter is particularly interesting in light of the experimental results on  $\text{Pr}_2\text{Ir}_2\text{O}_7$ , which shows a large AHE in a regime where the magnetization  $M$  is immeasurably small [11, 12]. On symmetry grounds,  $\sigma_{xy} \neq 0$  implies  $M_z \neq 0$ , but evidently  $\sigma_{xy}$  is unusually large relative to  $M$ . This behavior is in fact characteristic of the LAB: since the Hall conductivity has dimensions of inverse length, we expect  $\sigma_{xy} \sim H^{1/(z-\eta_{12})} \approx H^{0.51}$ . In the situation relevant for  $\text{Pr}_2\text{Ir}_2\text{O}_7$ , the Zeeman field is generated by Kondo exchange with the Pr moments, so  $H \sim J_K M$ , with  $M$  the (dimensionless) Pr magnetization, which implies a highly unconventional sublinear dependence of  $\sigma_{xy}$  on  $M$  for the pristine LAB. If the Fermi level is displaced from the band touching by an amount  $\epsilon_F$ , then we expect, treating the above power as a square root,  $\sigma_{xy} \sim \frac{e^2}{h} \sqrt{\frac{mH}{\hbar^2}} \mathcal{S}(H/\epsilon_F)$ , where  $\mathcal{S}$  is a scaling function (see Supp. Mat.). This gives an order of magnitude quantitative estimate

$$\sigma_{xy} \sim 10^3 \Omega^{-1} \text{cm}^{-1} \times \begin{cases} \sqrt{\frac{m}{m_e}} \sqrt{\frac{J_K}{\text{Ry}}} \sqrt{M}, & J_K M \gg \epsilon_F \\ \sqrt{\frac{m}{m_e}} \frac{J_K}{\epsilon_F \text{Ry}} M, & J_K M \ll \epsilon_F \end{cases}, \quad (7)$$

where  $\text{Ry}=13.6\text{eV}$  is the Rydberg, and  $m_e$  is the electron mass. The lower regime gives  $\sigma_{xy} \sim 0.1 \Omega^{-1} \text{cm}^{-1}$ , within an order of magnitude of observations in  $\text{Pr}_2\text{Ir}_2\text{O}_7$ , [12] for parameters  $m \sim 20m_e$  (estimated from the calculations in Ref. 15),  $\epsilon_F \sim 10\text{meV}$ ,  $J_K \sim 100\text{K}$  (estimated from the measured Curie-Weiss temperature), and  $M \sim 0.01$ .

Another interesting experimental observation in  $\text{Pr}_2\text{Ir}_2\text{O}_7$  is a diverging magnetic Gruneisen number  $\Gamma_H = \frac{1}{T} \frac{\partial T}{\partial H} \Big|_S$  in the zero field limit [29–31]. In a purely electronic system with no local moment contribution to the entropy, we can readily obtain the behavior of the LAB in the low temperature limit,

$$\Gamma_H(H, T) = -\frac{d - y_0 z}{y_0(z + \eta_H)} \frac{1}{H}, \quad (8)$$

which depends upon the exponent  $y_0$  defining the temperature dependence of the specific heat,  $C \sim T^{y_0}$ , of the LAB phase. In the Weyl metal,  $y_0 = 1$ , and  $\Gamma_H < 0$ , while for isolated double Weyl points,  $y_0 = 2$ , and  $\Gamma_H > 0$ . Thus one may imagine a sign change of the Gruneisen number when field or strain is varied. Note that in  $\text{Pr}_2\text{Ir}_2\text{O}_7$ , there is certainly a large local moment

contribution to the entropy, so that Eq. (8) is not literally applicable. Nevertheless, the LAB physics may play some role in this quantity.

In conclusion, we have described a novel NFL phase occurring in correlated strong SOC systems, with a natural connection to the pyrochlore iridates. Even with weak correlation effects, some of the phenomena discussed here can be observed with only minor modifications, and it would be interesting to search for them in  $\text{HgTe}$ . Future theoretical studies should include more comprehensive treatment of breaking of cubic symmetries, and the effects of disorder and doping.

We thank T. Hsieh, L. Fu, and P. Gegenwart for discussions on Luttinger model and Gruneisen number. This work was supported by NSF Grant DMR-1151208 and Hellman Family Foundation (EGM, CX), the David and Lucile Packard Foundation, the Alfred P. Sloan Foundation (CX), NSF-DMR-1206809 (LB), and NSERC, CIFAR (YBK). YBK and LB acknowledge the support and hospitality from the Aspen Center for Physics, funded by NSF grant PHY-1066293, and the KITP, funded by NSF grant PHY-1125915.

- 
- [1] L. Taillefer, *Annu. Rev. Cond. Mat.* **1**, 51 (2010).
  - [2] P.J. Hirschfeld, M.M. Korshunov, and I.I. Mazin, *Rep. Prog. Phys.* **74**, 124508 (2011).
  - [3] A. Chubukov, *Annu. Rev. Cond. Mat. Phys.* **3**, 57 (2012).
  - [4] P. Gegenwart *et al.*, *Nat. Phys.* **4**, 186 (2008).
  - [5] See, for example, M. Metlitski and S. Sachdev, *Phys. Rev. B* **82**, 075127 (2010); *ibid* 075128 (2010).
  - [6] D. Pesin and L. Balents, *Nat. Phys.* **6**, 376 (2010).
  - [7] B. J. Kim *et al.*, *Phys. Rev. Lett.*, **101**, 076402 (2008).
  - [8] B. J. Kim *et al.*, *Science* **323**, 1329 (2009).
  - [9] D. Yanagishima and Y. Maeno, *J. of Phys. Soc. Japan* **70**, 2880 (2001).
  - [10] K. Matsuhira *et al.*, *J. of Phys. Soc. Japan* **76**, 043706 (2007).
  - [11] S. Nakatsuji *et al.*, *Phys. Rev. Lett.* **96**, 087204 (2006).
  - [12] Y. Machida *et al.*, *Nature* **463**, 210 (2010).
  - [13] X. Wan *et al.*, *Phys. Rev. B*, **83**, 205101 (2011).
  - [14] W. Witczak-Krempa and Y. B. Kim, *Phys. Rev. B* **85**, 045124 (2012).
  - [15] B.-J. Yang and Y. B. Kim, *Phys. Rev. B* **82**, 085111 (2010).
  - [16] J. M. Luttinger, *Phys. Rev.* **102**, 1030 (1956).
  - [17] M. Z. Hasan and C. L. Kane, *Rev. Mod. Phys.* **82**, 3045 (2010).
  - [18] X.-L. Qi and S.-C. Zhang, *Rev. Mod. Phys.* **83**, 1057 (2011).
  - [19] B. A. Bernevig, T. L. Hughes, and S.-C. Zhang, *Science* **314**, 1757 (2006).
  - [20] M. König *et al.*, *Science* **318**, 766 (2007).
  - [21] A. A. Abrikosov and S. D. Beneslavskii, *Sov. Phys. JETP* **32**, 699 (1971).
  - [22] A. A. Abrikosov, *Sov. Phys. JETP* **39**, 709 (1974).
  - [23] S. Murakami, N. Nagaosa, and S.-C. Zhang, *Phys. Rev. B* **69**, 235206 (2004).

- [24] In this paper, we perform the  $\varepsilon = 4 - d$  expansion using the  $4 \times 4$  gamma matrices. Alternatively, one could use  $8 \times 8$  matrices in  $d = 4$  with a half of the number of fermion flavors and calculate logarithmic divergences directly.
- [25] B. I. Halperin and T. M. Rice, *Solid State Physics* **21**, 115 (1968).
- [26] L. Fu and C. Kane, *Phys. Rev. B* **76**, 045302 (2007).
- [27] B. J. Roman and A. W. Ewald, *Phys. Rev. B* **5**, 3914 (1972).
- [28] A. A. Burkov and L. Balents, *Phys. Rev. Lett.* **107**, 127205 (2011).
- [29] L. Zhu, *et al.*, *Phys. Rev. Lett.* **91**, 066404 (2003).
- [30] P. Gegenwart *et al.*, *J. Low Temp. Phys.* **161**, 117 (2010).
- [31] P. Gegenwart, private communication.

## SUPPLEMENTARY MATERIAL

### Representations of the Hamiltonian

In this section, we provide more information about the different representations used in the main text. The Hamiltonian reads

$$\begin{aligned} \mathcal{H}_0(k) &= \alpha_1 k^2 + \alpha_2 (\vec{k} \cdot \vec{J})^2 + \alpha_3 (k_x^2 J_x^2 + k_y^2 J_y^2 + k_z^2 J_z^2) \\ &= \frac{k^2}{2M_0} + \frac{(\frac{5}{4}k^2 - \vec{k} \cdot \vec{J})^2}{2m} - \frac{(k_x^2 J_x^2 + k_y^2 J_y^2 + k_z^2 J_z^2)}{2M_c} \\ &= \frac{d_a(k)}{2m} \Gamma^a + \frac{k^2}{2M_0} + \frac{d_4(k) \Gamma^4 + d_5(k) \Gamma^5}{2M_c}. \end{aligned} \quad (9)$$

The first line uses the conventional Luttinger parameters ( $\alpha_{1,2,3}$ ) in the  $j = 3/2$  matrix representation, and the second line is the form used in the main text. For the purpose of computations, it is convenient to introduce the Clifford gamma matrices ( $\Gamma_a$ ) in the third line as in the paper by Murakami *et al.* [23].

$$\begin{aligned} \epsilon_a(k) &= \frac{d_a(k)}{2m}, \\ d_1(k) &= -\sqrt{3}k_y k_z, \quad d_2(k) = -\sqrt{3}k_x k_z, \quad d_3(k) = -\sqrt{3}k_x k_y, \\ d_4(k) &= \frac{-\sqrt{3}}{2}(k_x^2 - k_y^2), \quad d_5(k) = \frac{-1}{2}(2k_z^2 - k_x^2 - k_y^2). \end{aligned} \quad (10)$$

It is straightforward to relate the masses used in the main text and the Luttinger  $\alpha_i$  parameters. This can be done by expressing the spin operators in terms of gamma matrices, using the equalities

$$\begin{aligned} J_x &= \frac{\sqrt{3}}{2} \Gamma_{15} - \frac{1}{2} (\Gamma_{23} - \Gamma_{14}), \\ J_y &= -\frac{\sqrt{3}}{2} \Gamma_{25} + \frac{1}{2} (\Gamma_{13} + \Gamma_{24}), \\ J_z &= -\Gamma_{34} - \frac{1}{2} \Gamma_{12}, \end{aligned} \quad (11)$$

where  $\Gamma_{ab} = \frac{1}{2i} [\Gamma_a, \Gamma_b]$  is used.

### Weyl semimetal

Here we consider how the Weyl semimetal appears, taking for simplicity the case  $\delta = 0, \theta_1 < \theta < \theta_2$ . It is straightforward to generalize this to the cases with  $\delta \neq 0$ . For convenience, we set  $m = 1/2$ . For  $\vec{k} = (0, 0, k_z)$ , the Hamiltonian in the presence of the Zeeman field,  $h$  (along the same axis), becomes

$$\mathcal{H}(k_z \hat{z}) = k_z^2 \left( \frac{5}{4} - J_z^2 \right) - H(\cos(\theta) J_z + \sin(\theta) J_z^3).$$

Clearly, the energy eigenstates can be labeled by both  $k_z$  and  $J_z = \pm 1/2, \pm 3/2$ . One can readily see that level crossings occur between the two bands with  $J_z = 1/2$  and  $J_z = -3/2$ . In the vicinity of these crossing points, the other states with  $J_z = -1/2, +3/2$  can be discarded, and the Hamiltonian projected onto the two level subspace of low energy states. We introduce Pauli matrices in this subspace, so that  $\tau^z = |\frac{1}{2}\rangle\langle\frac{1}{2}| - |-\frac{3}{2}\rangle\langle-\frac{3}{2}|$ ,  $\tau^+ = (\tau^x + i\tau^y)/2 = |\frac{1}{2}\rangle\langle-\frac{3}{2}| = (\tau^-)^\dagger$ , and  $\tau^0 = |\frac{1}{2}\rangle\langle\frac{1}{2}| + |-\frac{3}{2}\rangle\langle-\frac{3}{2}|$ , which is the identity matrix in the  $2 \times 2$  subspace. We define two energy parameters,  $\epsilon_{-3/2} = H(\frac{3}{2} \cos(\theta) + \frac{27}{8} \sin(\theta))$  and  $\epsilon_{1/2} = -H(\frac{1}{2} \cos(\theta) + \frac{1}{8} \sin(\theta))$ . Then the reduced Hamiltonian becomes

$$\begin{aligned} \mathcal{H}_2 &= \epsilon_+ \tau^0 + (\epsilon_- + d_5(k)) \tau^z + d_4(k) \tau^x - d_3(k) \tau^y, \\ \epsilon_{\pm} &= (\epsilon_{-3/2} \pm \epsilon_{1/2})/2. \end{aligned} \quad (12)$$

There are level crossing points at  $k_x = k_y = 0$  and  $k_z = \pm K$ , with  $K = \sqrt{\epsilon_-}$ . We expand around these points, letting  $k_x = p_x$ ,  $k_y = p_y$  and  $k_z = \pm K + p_z$ , which gives  $\mathcal{H}_2(\pm K \hat{z} + \vec{p}) = \epsilon_+ \tau^0 + \mathcal{H}_2^\pm(\vec{p})$ , with, to leading order in  $\vec{p}$ ,

$$\mathcal{H}_2^\pm = \mp v p_z \tau^z + d_4(p) \tau^x + d_3(p) \tau^y,$$

with  $v = 2\sqrt{\epsilon_-}$ . The energy spectrum is

$$E(p) = \pm \sqrt{v^2 p_z^2 + \frac{3}{4} (p_x^2 + p_y^2)^2}.$$

We see that the electrons disperse linearly along the field and quadratically orthogonal to it, near the touching point. This can be understood as a consequence of 4-fold rotational symmetry around the  $z$  axis. Since  $|J_z\rangle \rightarrow e^{i\pi J_z/2} |J_z\rangle$  under such a rotation, the operators  $\tau^\pm$  carry a net angular momentum of  $\pm 2$ , and therefore must couple to the “d-wave” combinations of  $p_x$  and  $p_y$ , which are precisely given by  $d_3(p)$  and  $d_4(p)$ .

Though the quadratic dispersion normal to the field is due to symmetry, the touching itself has a topological character. To see it, it is convenient to define the reduced Hamiltonian in the form

$$\mathcal{H}_2^\pm = \vec{b}_\pm(\vec{p}) \cdot \vec{\tau}, \quad (13)$$

with

$$\vec{b}_\pm(\vec{p}) = \begin{pmatrix} -\frac{\sqrt{3}}{2}(p_x^2 - p_y^2) \\ \sqrt{3}p_x p_y \\ \mp v p_z \end{pmatrix}. \quad (14)$$

From this, one can define the  $U(1)$  Berry flux, which is analogous to a magnetic field in momentum space,

$$\mathcal{B}_\pm^\mu = \frac{1}{8\pi} \epsilon^{\mu\nu\lambda} \hat{b}_\pm \cdot \partial_\nu \hat{b}_\pm \times \partial_\lambda \hat{b}_\pm, \quad (15)$$

where  $\hat{b}_\pm = \vec{b}_\pm / |\vec{b}_\pm|$ , and the derivatives are with respect to  $\vec{p}$ . By construction, the magnetic field is divergenceless,  $\partial_\mu \mathcal{B}_\pm^\mu = 0$ , away from points of singularity where  $\vec{b}_\pm$  vanishes. However, the band touching point is such a singularity, and it is in fact a source of Berry flux. To see this, one may compute the integral of the flux of  $\mathcal{B}^\mu$  through a sphere around one of the touching points. It is straightforward to compute this integral, and by doing so one finds

$$\partial_\mu \mathcal{B}^\mu(\vec{p}) = \pm 2\delta(\vec{p}). \quad (16)$$

Thus each band touching is a source of *two* quanta of Berry flux, and can be therefore considered a *double Weyl point*. The net Berry flux of both double Weyl points added together vanishes, which is required as the Brillouin zone is a closed manifold without any boundary through which a net flux may escape.

The Berry flux of each double Weyl point is directly related to the Hall conductivity. Indeed, one can show quite generally that the Hall conductivity is proportional to separation of the points,[28]

$$\sigma_{xy} = 2 \times \frac{e^2}{h} \times \frac{2K}{2\pi},$$

where the first factor of 2 is due to the doubled nature of the Weyl points. This is valid at zero temperature when the Fermi level is at the energy of the double Weyl points. Neglecting the small corrections to the exponent due to Coulomb interactions, we have  $K \sim \sqrt{mH}$ , which explains the estimate in Eq. (7) of the main text.

### RG equations

Here we describe the renormalization of the fermionic propagator, which was not presented in the main text. We start with the Hamiltonian

$$\mathcal{H}_0(k) = \frac{k^2}{2M_0} \Gamma^0 + \epsilon_a(k) \Gamma^a + \frac{d_4(k) \Gamma^4 + d_5(k) \Gamma^5}{2M_c},$$

where we defined  $\Gamma^0$  as the  $4 \times 4$  unit matrix to emphasize the matrix structure. The corresponding effective

Lagrange density is

$$\mathcal{L}_{\text{eff}} = \psi^\dagger (-i\omega_n \Gamma^0 + \mathcal{H}_0(k) - \Sigma_f(k, i\omega_n)) \psi.$$

Here we have included the one-loop self energy needed for the  $\varepsilon$  expansion. It is given by

$$\Sigma_\psi(k, i\omega_n) = -g^2 \int_q T \sum_{\Omega_n} G_f(k+q, i\omega_n + i\Omega_n) G_\varphi(q, i\Omega_n), \quad (17)$$

where  $G_f^{-1}(k, i\omega) = -i\omega \Gamma^0 + \mathcal{H}_0(k)$ ,  $G_\varphi^{-1}(q, i\Omega) = c_0 q^2$  are used. Note that the bosonic propagator does not have frequency dependence since it represents the instantaneous Coulomb interaction. By integrating out high momentum degrees of freedom, we investigate the renormalization of fermion parameters.

Frequency and momentum dependences of the self energy determine anomalous dimensions of the fermion field and mass terms, respectively. At one-loop level, the fermion self energy does not have frequency dependence due to the instantaneous Coulomb interaction, so no anomalous dimension of the fermion field appears. Moreover, the frequency-independence makes one mass coupling ( $1/M_0$ ) unchanged at one loop level and it is because frequency and this mass term have the same unity matrix structure. Note that both corrections naturally appear in higher-loop contributions.

On the other hand, non-trivial renormalizations of isotropic mass ( $m$ ) and anisotropic mass ( $M_c$ ) appear even at one-loop level. For example, the renormalization of isotropic mass term can be read off by calculating the third component ( $\Gamma^3$ ) of the self energy,

$$\begin{aligned} \gamma^3(k) &\equiv \text{Tr} \left( \Gamma^3 \frac{\partial^2}{\partial k_x \partial k_y} \Sigma_\psi(k, 0) \right) / \text{Tr}(\Gamma^3 \Gamma^3) \\ &= -\frac{g^2}{c_0} \frac{\partial}{\partial k_x \partial k_y} \int_q \frac{\epsilon_3(k+q)}{\sqrt{\left(\frac{(k+q)^2}{2m}\right)^2 + \frac{m+2M_c}{4mM_c} p_c(k+q)}} \frac{1}{q^2}. \end{aligned}$$

It can be understood as the self energy correction to the original Hamiltonian,

$$\begin{aligned} \epsilon_3(k) &\rightarrow \epsilon_3(k) - \gamma^3(0) k_x k_y \\ &= \epsilon_3(k) \left( 1 + u f_1\left(\frac{m}{M_c}\right) \log\left(\frac{\Lambda}{\mu}\right) \right). \end{aligned} \quad (18)$$

In the last line, the momentum integration is done for  $\mu < q < \Lambda$ . The correction to the isotropic mass term,  $\delta(1/m) = \frac{u}{m} f_1\left(\frac{m}{M_c}\right) \log\left(\frac{\Lambda}{\mu}\right)$  can be regularized in the standard way. Along the same line, one can determine the renormalization of the anisotropic mass term by calculating the fourth component ( $\Gamma^4$ ) of the self-energy.

These considerations lead to the full RG equations as

follows.

$$\begin{aligned} \frac{d}{dl} \left( \frac{1}{m} \right) &= \left( z - 2 + u f_1 \left( \frac{m}{M_c} \right) \right) \left( \frac{1}{m} \right), \\ \frac{d}{dl} \left( \frac{m}{M_0} \right) &= -u f_1 \left( \frac{m}{M_c} \right) \frac{m}{M_0}, \\ \frac{d}{dl} \left( \frac{m}{M_c} \right) &= -u F_2 \left( \frac{m}{M_c} \right), \\ \frac{d}{dl} (u) &= \varepsilon u - N_f F_1 \left( \frac{m}{M_c} \right) u^2. \end{aligned}$$

Here the following functions of anisotropy are introduced.

$$\begin{aligned} f_1(x) &= \frac{2}{\pi} \int d\Omega_k \frac{\hat{k}_x^2 \hat{k}_y^2}{\sqrt{1 + x(2+x)p_c(\hat{k})}}, \\ f_2(x) &= \frac{1}{2\pi} \int d\Omega_k \frac{(\hat{k}_x^2 - \hat{k}_y^2)^2}{\sqrt{1 + x(2+x)p_c(\hat{k})}}, \\ f_3(x) &= \frac{3}{8\pi} \int d\Omega_k \frac{x^4 \hat{k}_x^2 (\hat{k}_y^2 - \hat{k}_z^2)^2}{\left( \sqrt{1 + x(2+x)p_c(\hat{k})} \right)^5} + O\left(\frac{1}{x}\right), \\ F_1(x) &= 2f_3(x) + \frac{1}{N_f} f_1(x), \\ F_2(x) &= (1+x)(f_1(x) - f_2(x)), \end{aligned}$$

where  $p_c(k) = \sum_{i=1}^3 k_i^4 - \sum_{i \neq j} k_i^2 k_j^2$  is used. The first two functions,  $f_1$  and  $f_2$ , are from the fermion self energy and the third function,  $f_3$ , is from the boson self-energy calculation. The asymptotic form of  $f_3$  is shown above while its complete form can be obtained by evaluating the bosonic self energy function directly. Numerical evaluations of these functions are illustrated in Figs. 2 and 3. Useful numerical values are

$$\begin{aligned} N_f F_1(0) &= \frac{30N_f + 8}{15}, \quad F_2(0) = 0, \quad F_2'(0) \sim 0.152, \\ f_1(0) = f_2(0) &= \frac{8}{15}, \quad f_3(0) = 1, \\ \lim_{x \rightarrow \infty} f_1(x) &= \lim_{x \rightarrow \infty} f_2(x) = 0, \\ \lim_{x \rightarrow \infty} f_3(x) &\sim 0.888. \end{aligned}$$

We note that there is one subtle issue in the  $\varepsilon$  expansion for regularization of the loop corrections. Since the gamma matrices are defined in specific dimensions, there is some ambiguity for the choice of gamma matrices in dimensional regularization. There have been some sug-

gestions as to how to apply the  $\varepsilon$  expansion to Gamma matrices. [22]

In this letter, we use one of possible regularization schemes; the angle dependence is first integrated in the original dimension and then dimensional regularization is used for the integrals over the magnitude of momentum. One reason for using this scheme is our need to keep track of the cubic anisotropy, which is specifically defined

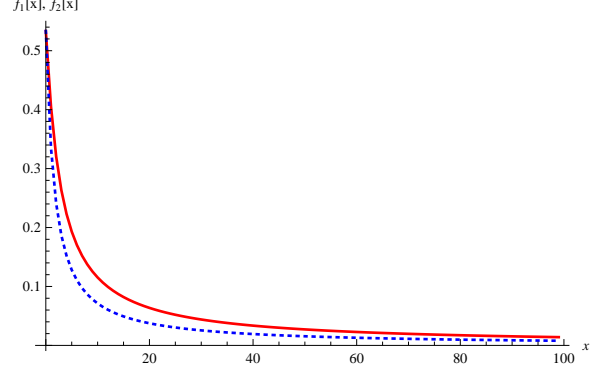


FIG. 2. Numerical evaluations of the renormalization functions,  $f_1(x), f_2(x)$ . The solid (red) and dotted (blue) lines are for  $f_1(x)$  and  $f_2(x)$  ( $f_1(0) = f_2(0) = 8/15$ ). One can show that  $f_1(x) - f_2(x)$  decays as  $1/x$  in the large  $x$  limit.

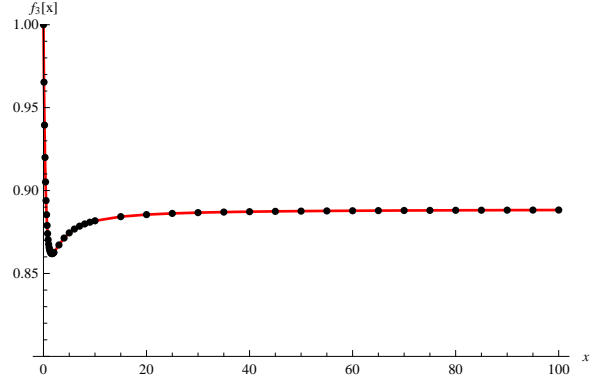


FIG. 3. Numerical evaluations of the universal function,  $f_3(x)$ . One can see that  $f_3(x)$  becomes saturated as  $x$  becomes large.

in three spatial dimensions. Formally, the momentum shell integration gives  $\int_{\Lambda}^{\Lambda} e^{-dl} \frac{d^d q}{(2\pi)^d} \frac{1}{q^4} \rightarrow \frac{dl}{8\pi^2}$ . Note that different regularization schemes only change numerical coefficients and do not change important physics.